Evolution with annealing of solar cell parameters modeling the S-shape of the current–voltage characteristic

G. del Pozo, B. Romero*, B. Arredondo

Departamento Tecnología Electrónica, Universidad Rey Juan Carlos, C/ Tulipán s/n, 28933 Móstoles, Madrid, Spain

Keywords:
Modeling
Organic solar cell
Annealing

A B S T R A C T

In this work we use a modified equivalent circuit to simulate the S-shape found in current density–voltage (J–V) characteristics of organic solar cells (OSC) based on P3HT:PCBM. The modification of the traditional model includes a second diode opposite to the main one together with a parallel resistance, R_{P2}. The transcendental equation derived from the circuit is solved exactly without approximations. The S-shape (so called kink), usually attributed to a poor quality of polymer/cathode interface, can be removed after three slow annealing treatments. The evolution of the J–V curves with the annealing process has been quantified by extracting the equivalent circuit parameters of each curve (pristine and annealed) by fitting the model to the experimental data. Results show that kink annihilation is mostly due to a strong decrease of R_{P2}, which diminishes the reverse diode effect on the J–V curve.

1. Introduction

The recent major development of conjugated polymers [1], together with the discovery of photoinduced charge transfer at donor–acceptor interface in organic materials [2] have generated a great interest in organic photovoltaic devices. Organic solar cells appear as a promising alternative to conventional inorganic photovoltaic devices with potential advantages such as: low-cost and ease of processing, integration onto unconventional substrates, and the existence of a vast variety of organic structures whose functionalities can be chemically tuned to adjust the energy levels and therefore improve light absorption and charge transport. Critical issues to assure a good operation in organic solar cells can be summarized as follows: (1) absorption of photons in the polymer active layer to create excitons, (2) diffusion of excitons to the donor–acceptor (D/A) interface, (3) exciton dissociation at the interface to create polaron pairs, (4) separation of carriers under the electric field produced by the anode/cathode workfunction difference, and (5) transport of free charges to their respective electrodes. In bilayer solar cells, only a small fraction of photo-generated excitons can reach the D/A interface, since typical exciton diffusion length is smaller than the required thickness for efficient light absorption. This problem can be overcome using blends as active layer. These blends are composed of a donor polymer and an acceptor molecule to form a bulk composite consisting of an interpenetrating network of D/A materials with nanoscale heterojunction interfaces. This bulk heterojunction (BHJ) solar cell ensures that all photogenerated excitons reach a D/A interface within the diffusion length. Among all possible combinations of D/A pairs, P3HT-PCBM is a well studied system with power conversion efficiency (PCE) reaching up to 5% [3–5] and 6% for a tandem cell geometry [6].

On the other hand, too fine scale mixing makes charge collection difficult since each material must provide continuous pathways for charges to be transported, resulting in a decrease of mobility and an increase of series resistance. Therefore, a trade-off between exciton dissociation and charge transport is pursued. In this sense, bulk morphology plays an important role in charge transport in BHJ solar cells, and it can be controlled by playing with factors such as the solvent, drying conditions or device annealing [7–10]. In particular, many studies have been focused on device annealing, since it enhances crystallinity, thus, improving carrier mobility and reducing internal resistance [11,12].

Besides morphology, organic–electrode interface critically influences device performance. A typical phenomenon in BHJ solar cells is the appearance of a "kink" or S-shape in the J–V characteristic. This feature results in a reduced fill-factor (FF) and thus, a decreased solar cell efficiency. In fact, FF is more sensitive to the polymer–electrode interface than other parameters such as open-circuit voltage (V_{OC}) or short-circuit current (I_{SC}). The origin of the kink is still a matter of continuous research [13–19]. Previous studies suggest that low quality interfaces attributed to cathode evaporation under realistic conditions may lead to a variety of chemical and physical defects that can be detrimental [16–18,20]. These authors relate the curvature of the J–V characteristic in the fourth quadrant to the FF, showing J–V convex curvature for devices with FF > 50% and concave shape corresponding to FF < 12.5%. The kink-shape has also been observed in roll to roll devices fabricated in ambient air with a ZnO hole transport layer, where this phenomenon has been attributed to a

* Corresponding author. Tel.: +34 91 488 7178; fax: +34 91 488 7049.
E-mail address: Beatriz.romero@urjc.es (B. Romero).

redistribution of oxygen within the device [21]. According to these authors, the appearance of S-shape is a dynamic process that can be removed under photo-annealing treatment. Moreover, device degradation studies using TOF-SIMS imaging reveal that oxygen diffusion into the device through the Al cathode until the counter electrode is the responsible mechanism for this anomalous shape [22]. Other strategies to avoid S-shape are the insertion of a bathocuproine (BCP) buffer layer between active layer and Al contact [13], and doping the zinc oxide layer with aluminum [23]. Moreover, some authors propose the formation of traps at the interface due to the presence of Al nanoclusters in the organic layer formed during cathode evaporation [19,24]. These traps are responsible for a change in the electric field distribution inside the device, screening the electric field at the interface and leading to the observed kink. When devices undergo an annealing process, these Al nanoclusters eventually merge with the cathode, smoothing the S-shape from the *J–V* characteristic and ultimately disappearing. In addition, charge space effects leading to unbalanced charge transport and carrier accumulation at the interfaces can also be a second order cause of the appearance of the S-shape. Recent theoretical studies attributed the S-kink to a hole–electron mobility mismatch factor larger than 100 [25].

Even though physical processes taking place in inorganic and organic solar cells are quite different, conventional circuit modeling employed in inorganic cells [26] has often been used in organic ones. These circuital models have been useful to extract device parameters using approximated solutions to the circuit equations [27–30] or obtaining the analytical exact solutions using Lambert W-function [31–33]. The main difference between inorganic and organic solar cells is that after light absorption, instead of free carriers, excitons are created and diffused to the nearest D/A interface to form polaron pairs. Mazhari revised the validity of the traditional circuit and introduced modifications to model the physical processes taking place in organic semiconductors [34]. Furthermore, Castro et al. proposed a modified solar cell equivalent circuit to simulate the appearance of the S-shape in the *J–V* characteristic of MEH-PPV-C_{60} solar cells. They introduced a second diode in reverse bias operation to simulate the effect of traps at the interface, and solve the rather complex circuit equations in an approximate way by introducing two effective resistances and neglecting single diode currents vs. the total input device current [19]. However, this approximation does not hold for all bias, and therefore it leads to a solution that may not be valid in the whole current–voltage operation range.

In this work we fabricate P3HT:PCBM blend solar cells to report on the evolution of the kink in the *J–V* curve for as-casted devices and after undergoing several annealing processes. The goal of this work is to simulate this non-ideal behavior that can affect dramatically the solar cell performance and study the evolution of the circuital parameters. The physical phenomena occurring at the interface responsible for this shape in the *J–V* are beyond the scope of this work. We have adopted the model proposed by Castro et al. to simulate the S-shape in the *J–V* curve. We solve the circuit without approximations to obtain an exact solution for current and voltage, and thus, extract reliable values for circuital parameters: R_S, R_{P1}, R_{P2}, J_{01} and J_{02}. These parameters are obtained as function of the number of annealing process. We find that approximations methods to solve the circuit may lead to inconsistent parameters values.

2. Experimental details

Patterned indium tin oxide (ITO) glass substrates were cleaned by ultrasonic treatment in different baths with distilled water, acetone and iso-propanol and subsequently dried with N_2 flow. Substrates were exposed for 30 min to UV irradiation. A hole transport layer of highly conductive poly(3,4-ethylenedioxythiophene)-poly(4-styrene sulfonate)(PEDOT:PSS) from aqueous solution was spin-coated and annealed in oven for 30 min at 110 °C to obtain a ~50 nm layer thickness. The active layer was spin-coated from an anhydrous chlorobenzene (CB) solution composed by a P3HT:PCBM blend. The P3HT:PCBM ratio was set to 1:1 and the solution concentration was 46.7 mg mL^{-1} (~4% wt). Solutions were stirred for several hours and spin-coated at 1000 rpm to obtain a ~260 nm active layer thickness. Samples were dried in an oven at 75 °C for 2 h before cathode deposition in order to remove any solvent residue. Next, an Al cathode was thermally evaporated on top of the active layer through a shadow mask in an atmosphere of 10^{-6} Torr. Finally, devices were encapsulated using a glass cover attached by an epoxy adhesive in order to minimize degradation. All processes were carried out in a glove box with inert atmosphere with low levels of H_2O and O_2 (< 0.1 ppm) except for the cathode evaporation. Active area of the resulting devices was 0.07 cm^2.

Current–voltage characteristics were carried out with a Semiconductor Parameter Analyzer Agilent 4155C and source generator Agilent 41501B. Cells were illuminated with a halogen lamp with a power density of 400 W m^{-2}.

In order to study the effect of the thermal annealing, devices were subjected to a slow annealing process, which consists of rising the temperature of the hot plate from 25 °C to 100 °C in four steps during 90 min approximately (30 min at 50 °C, 30 min at 75 °C and 30 min at 100 °C). This treatment was carried out until the kink in the *J–V* curve was completely removed. After each annealing, samples were cooled down to room temperature before measuring the *J–V* curve.

3. Results and discussion

3.1. Circuit model

Fig. 1 shows conventional and simple equivalent circuit for solar cells. I_L represents the photo-generated current density, $d1$ is a diode that takes into account the non-linear behavior of organic solar cells, R_{S1} is the series resistance and R_{P1} is the parallel resistance. Eq. (1) is derived by applying Kirchhoff's laws to the mentioned circuit:

$$I = I_{d1} + I_{RP1} - I_L = I_{01}[\exp(\alpha_1 V_d) - 1] + \frac{V_d}{R_{P1}} - I_L \quad (1)$$

where V_d is the voltage drop across the diode and is given by $V_d = V - R_{S1}I$, I_{01} is the diode saturation current and $\alpha_1 = q/n_1 KT$, where n_1 is the diode ideality factor, q is the electron charge, K is the Boltzmann constant and T is the absolute temperature. Using this simple model, it is possible to reproduce typical organic solar cells behavior under dark (I_L=0) and illumination conditions. However, when the S-shape appears in the *J–V* curve, this model cannot reproduce the entire curve. Castro et al. proposed a more complex circuit that reproduces S-shape by adding a second diode with a second parallel resistance, as shown in Fig. 2 [19]. In this model, the first diode is working under forward bias and is responsible for the

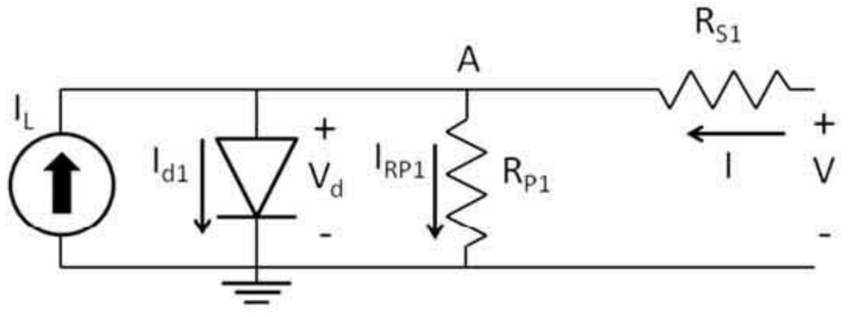

Fig. 1. Conventional equivalent circuit of organic solar cells.

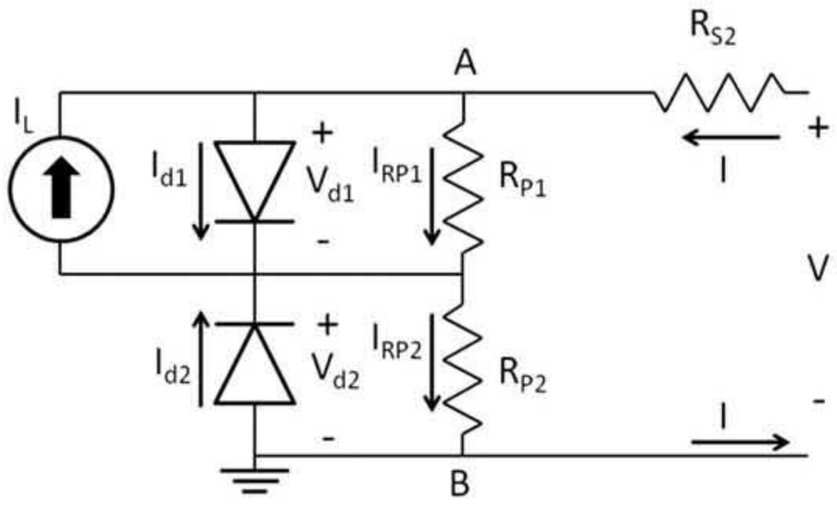

Fig. 2. Modified equivalent circuit including a new element (diode 2) opposite to the solar cell diode (diode 1).

exponential behavior of the *J–V* curve. The second diode is placed opposite to the first one and is essential to simulate the S-shape appearing in the *J–V* curve. The main contribution of this diode is to simulate the non-ideal effects of active layer/cathode interface. These deviations from ideality can be due to any physical process that leads to a change in the electric field distribution in the device. The origin of these physical changes is beyond the scope of this paper. Some authors attribute it to the incorporation of Al nanoclusters in the organic layers during evaporation [19] while others point out the effect of polarons at the interface [17].

Applying Kirchhoff's voltage law (KVL) in circuit of Fig. 2, we can obtain the following expression relating voltage and current.

$$V = R_{S2}I + V_{d1} + V_{d2} = R_{S2}I + R_{P1}I_{R_{P1}} + R_{P2}I_{R_{P2}} \tag{2}$$

where V_{d1} and V_{d2} are the voltage drops across parallel resistances R_{P1} and R_{P2} respectively, and $I_{R_{P1}}$ and $I_{R_{P2}}$ are the currents flowing through them. On the other hand, applying Kirchhoff's current law (KCL) in node A, we obtain:

$$I_{R_{P1}} = I + I_L - I_{d1} \tag{3}$$

where I_{d1} is the current through the diode 1 and is given by the following equation:

$$I_{d1} = I_{01}[\exp(\alpha_1 V_{d1}) - 1] \tag{4}$$

Applying KCL in node B we obtain Eq. (5).

$$I_{R_{P2}} = I + I_{d2} \tag{5}$$

where the current through the diode 2, I_{d2}, is given by the equation:

$$I_{d2} = I_{02}[\exp(-\alpha_2 V_{d2}) - 1] \tag{6}$$

From Eqs. (2) and (5) we can obtain the following expresion for V_{d1}:

$$V_{d1} = V - R_{S2}I - R_{P2}I_{R_{P2}} = V - R_{S2}I - R_{P2}(I + I_{d2}) \tag{7}$$

Following the same procedure with Eqs. (2) and (3) we obtain the following expression for V_{d2}.

$$V_{d2} = V - R_{S2}I - R_{P1}I_{R_{P1}} = V - R_{S2}I - R_{P1}(I - I_{d1} + I_L) \tag{8}$$

Substituting expressions (7) and (8) in Eqs. (4) and (6) respectively, we obtain the following expressions for I_{d1} and I_{d2}:

$$I_{d1} = I_{01}\{\exp[\alpha_1(V - R_{S2}I - R_{P2}I - R_{P2}I_{d2})] - 1\} \tag{9}$$

$$I_{d2} = I_{02}\{\exp[-\alpha_2(V - R_{S2}I - R_{P1}I + R_{P1}I_{d1} - R_{P1}I_L)] - 1\} \tag{10}$$

Moreover, substituting expressions (3) and (5) in Eq. (2) leads to

$$V = R_{S2}I + R_{P1}(I + I_L - I_{d1}) + R_{P2}(I + I_{d2}) \tag{11}$$

Finally, Eq. (11) can be rewritten as

$$(R_{P1} + R_{P2})I = (V - R_{S2}I) + R_{P1}I_{d1} - R_{P2}I_{d2} - R_{P1}I_L \tag{12}$$

It is worth noticing that when $I_{02}=0$ or $R_{P2}=0$, circuit in Fig. 2 is reduced to the simplest circuit in Fig. 1 with $R_{S1} = R_{P2} + R_{S2}$. In that case, Eq. (1) can be solved analytically using W-Lambert functions or numerical methods [31–33].

In a more general case we need to solve the system of equations given by (9), (10) and (12). It can be seen that I_{d2} appears in the exponential factor of I_{d1} (Eq. (9)) and vice versa (Eq. (10)). This results in a transcendental system of equations that we have solved using numerical methods. In this context, some authors use approximations in order to simplify the equation system. Castro et al. reduced Eqs. (9) and (10) by neglecting the terms I_{d2} and I_{d1} in the exponential factors of I_{d1} (Eq. 9) and I_{d2} (Eq. 10) respectively, and introducing two effective resistances [19]. Nevertheless, we have found that solutions obtained doing these simplifications are not always valid for the entire regime.

In order to study the validity of these simplifications, we have simulated a *J–V* curve with S-shape by solving the above equations without any approximation. The parameters used to generate the S-shape are fixed to $R_{P1}=0.7$ MΩ, $R_{P2}=6.0$ kΩ, $R_S=0.0$ Ω, $I_{01}=9.8$ μA, $I_{02}=29.4$ μA, $n_1=6.5$, $n_2=3.0$ and $I_L=77.0$ μA. We have calculated the currents through the first and second diode and we have found that none of the currents can be neglected when compared to the total current for the entire regime. In the Fig. 3, current densities J, J_{d1} and J_{d2} are plotted against voltage in order to compare them.

3.2. Numerical procedure

As shown above, solving electric circuit with two diodes leads to a transcendental system of equations that has to be solved using numerical methods. Even so, finding out a solution is not an easy task.

The equation system has been solved as follows: substituting (4) and (6) in Eqs. (3) and (5) respectively leads to

$$I = I_{d1} + I_{R_{P1}} - I_L = I_{01}\{\exp(\alpha_1 V_{d1}) - 1\} + \frac{V_{d1}}{R_{P1}} - I_L \tag{13}$$

$$I = -I_{d2} + I_{R_{P2}} = -I_{02}\{\exp(-\alpha_2 V_{d2}) - 1\} + \frac{V_{d2}}{R_{P2}} \tag{14}$$

from Eqs. (13) and (14), we obtain V_{d1} and V_{d2} for a given current by numerically solving each equation separately. Once we know the voltage across each diode, the total voltage is given by Eq. (2).

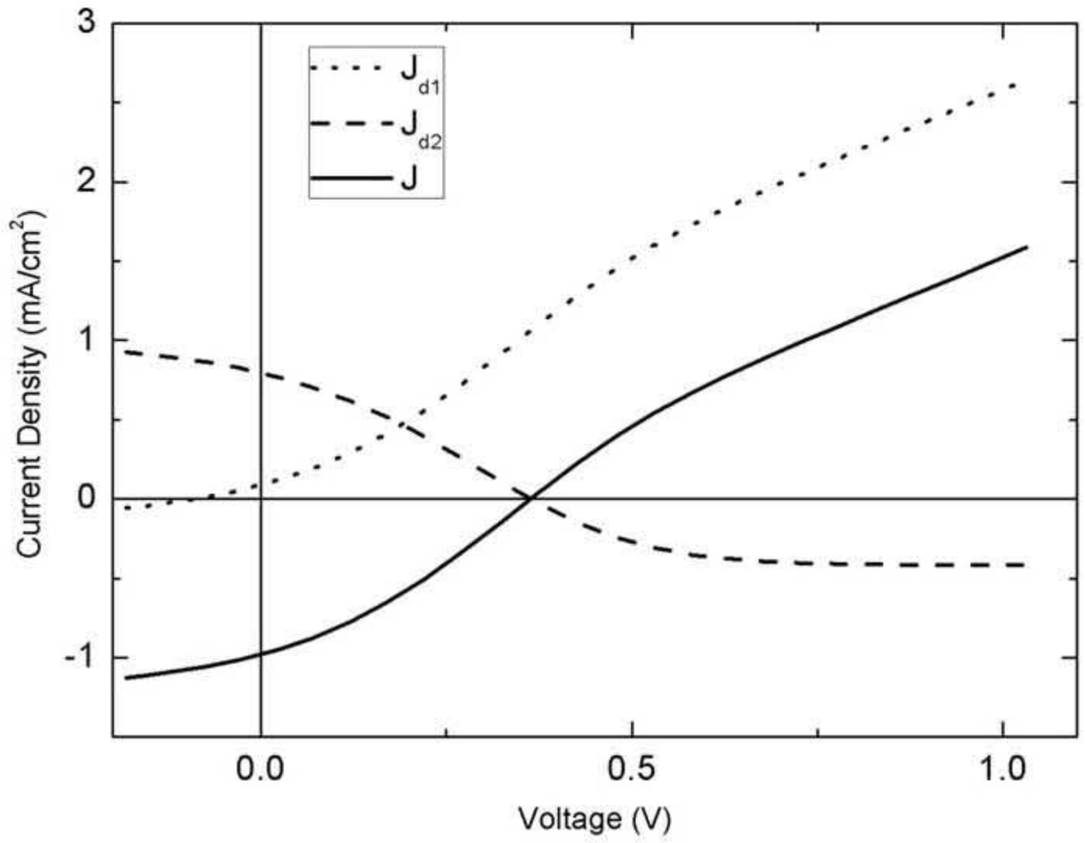

Fig. 3. Simulated diode current densities and total current density vs. voltage.

The Appendix A shows the corresponding flow diagram followed to generate a J–V curve for a given set of parameters. It is worth mentioning that when using this algorithm the control parameter is the current instead of voltage.

3.3. Theoretical simulations

In order to show the influence of the diode 2 in the J–V curve, different curves varying J_{02} and R_{P2} have been simulated (Fig. 4). The remaining parameters have been set to the same values as in Fig. 3 so as to ensure the S-shape in the initial J–V curves.

When J_{02} is either very low or very high, circuit 2 becomes circuit 1. When J_{02} is very small, the dynamic diode resistance is very high resembling an open circuit. In this case no current flows through diode 2 and effect of R_{P2} is equivalent to that of a series resistance. Then total series resistance in the circuit is $R_{S2}+R_{P2}$. On the other hand if J_{02} is very high, the dynamic diode resistance is very low which causes all the current flowing through diode 2 and no current through R_{P2}. In the limit $J_{02}\rightarrow\infty$, the diode behaves as a short circuit, and circuit 2 becomes circuit 1. In this case total series resistance is R_{S2}. In the intermediate case, the effect of diode 2 is to produce a kink in J–V curve. In Fig. 4a several simulations are shown. Starting from J_{02}=0.86 mA cm^{-2} (solid line) the S-shape is well pronounced. Then, J_{02} is gradually decreased in order to verify the extinction of the kink and the increase in total series resistance. This behavior is shown in Fig. 4a where different J–V curves are plotted for different values of J_{02}.

Fig. 4b shows that a decrease of R_{P2} increases the total current flowing through R_{P2}. In the limit $R_{P2}\rightarrow 0$, this resistance is much lower than dynamic diode resistance, and diode 2 resembles an open circuit. In this case, circuit 2 becomes circuit 1 with total series resistance $R_{S1}\approx R_{S2}+R_{P2}$. Fig. 4b shows the evolution of the kink shape, when R_{P2} is decreased from 25.6 kΩ, down to 1.6 kΩ.The kink disappears and total series resistance decreases.

3.4. Validation of the model

To validate the proposed model, theoretical simulations have been fitted to experimental J–V curves of devices showing different degrees of S-shape. Starting with a pristine device showing S-shape, it was undergone to three annealing processes that removed the kink completely.

As mentioned before, the control parameter in the J–V generation algorithm is current instead of voltage. Therefore, the error used to obtain the best fit is defined as the difference between the experimental and the calculated voltage (Eq. (15)).

$$Error=\sum|V_{CALC}-V_{EXP}| \tag{15}$$

In order to limit the computational time we have reduced the number of free parameters. After the first few fittings we have discovered that the role of R_{S2} can be included in R_{P2}, simplifying the fitting process. Ideality factors n_1 and n_2 have been fixed to 6.5 and 3.0 respectively since those were the values more repeated in the best fits. These values are in good agreement with those found in the literature for organic devices [29,35,36]. In the proposed model, I_L is assumed to depend just on the illumination level but not on the bias voltage. We can assume that when no voltage is applied to the OSC, all the measured current is photogenerated. This current is named short-circuit current (I_{SC}). Therefore, we have restricted I_L to a value very close to experimental I_{SC}.

Finally, simulations were performed leaving as free parameters R_{P1}, R_{P2}, J_{01} and J_{02}. The model has been fitted to experimental curves of devices that have undergone increasing annealing treatments, and show different degrees of S-shape (Fig. 5).

The fitting procedure has been performed using a non-deterministic genetic algorithm. This kind of algorithms is considered to be particularly suitable for systems with many parameters, achieving reliable results with significant reduction in computing time [37]. Fig. 5 shows that best fits obtained are very good both in linear and logarithmic scale (inset) in the whole studied range (from −0.2 V to 1.0 V). The average square error obtained from the fits is always less than 4%, indicating a good agreement between theoretical and experimental data.

Table 1 shows the evolution of the FF, PCE and electric parameters extracted for each J–V curve. A FF enhancement from 0.32 to 0.36 after the first annealing is reflected in the kink removal as can be seen in Fig. 5. As a consequence, PCE increases up to 50%. Subsequent annealings do not vary significantly the solar cell parameters. Regarding circuital parameters, J_{02} changes from 0.42 mA cm^{-2} to 0.28 mA cm^{-2} while R_{P2} decreases from 6.44 kΩ to 1.47 kΩ after the three annealing processes. As explained in Section 3, both trends decrease S-shape as expected. It should be noted that in the first annealing, the decrease in R_{P2} is

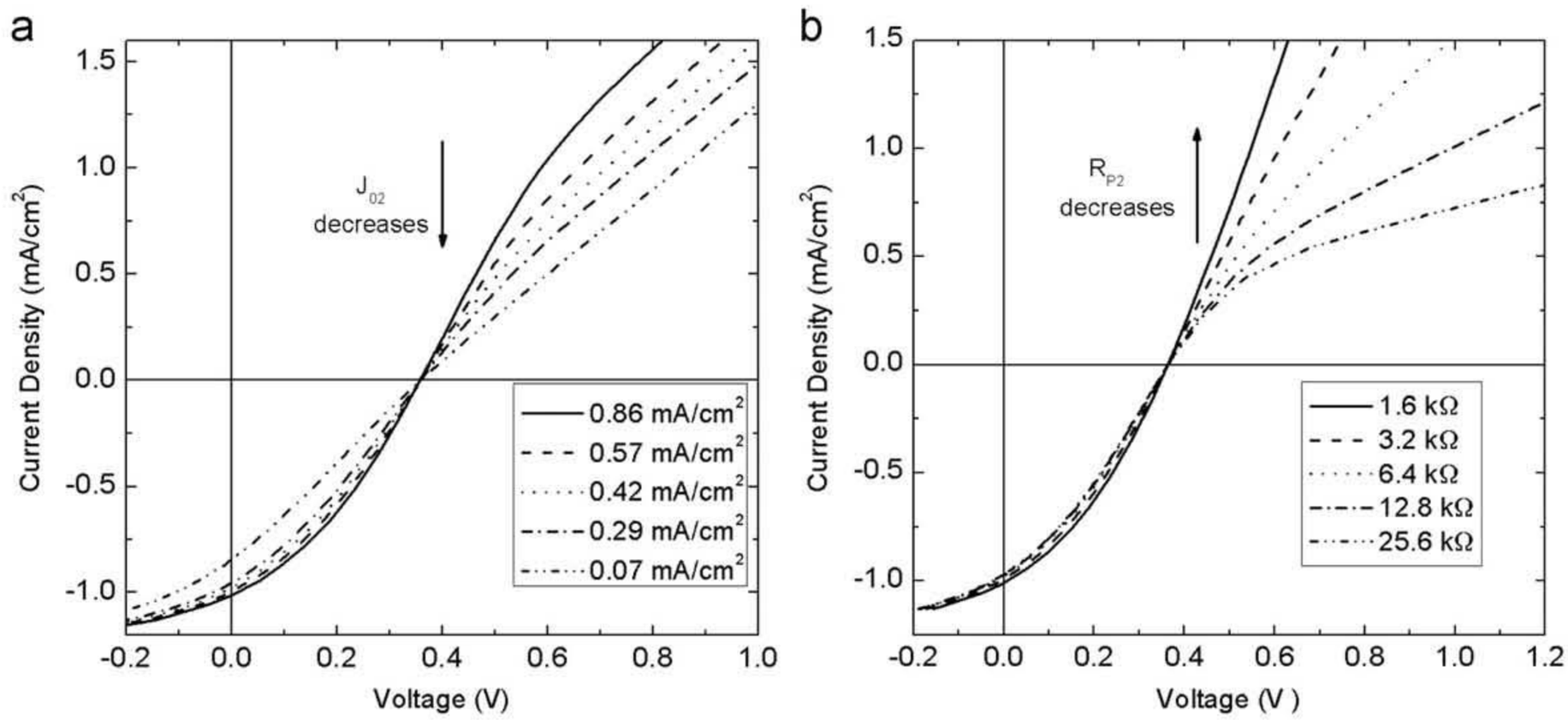

Fig. 4. Theoretical J–V curves varying J_{02} (left) and R_{P2} (right). (R_{P1}=0.7 MΩ; R_S=0 Ω; J_{01}=0.14 mA cm ^{2}; n_1=6.5; n_2=3.0; J_L=1.1 mA cm ^{2}).

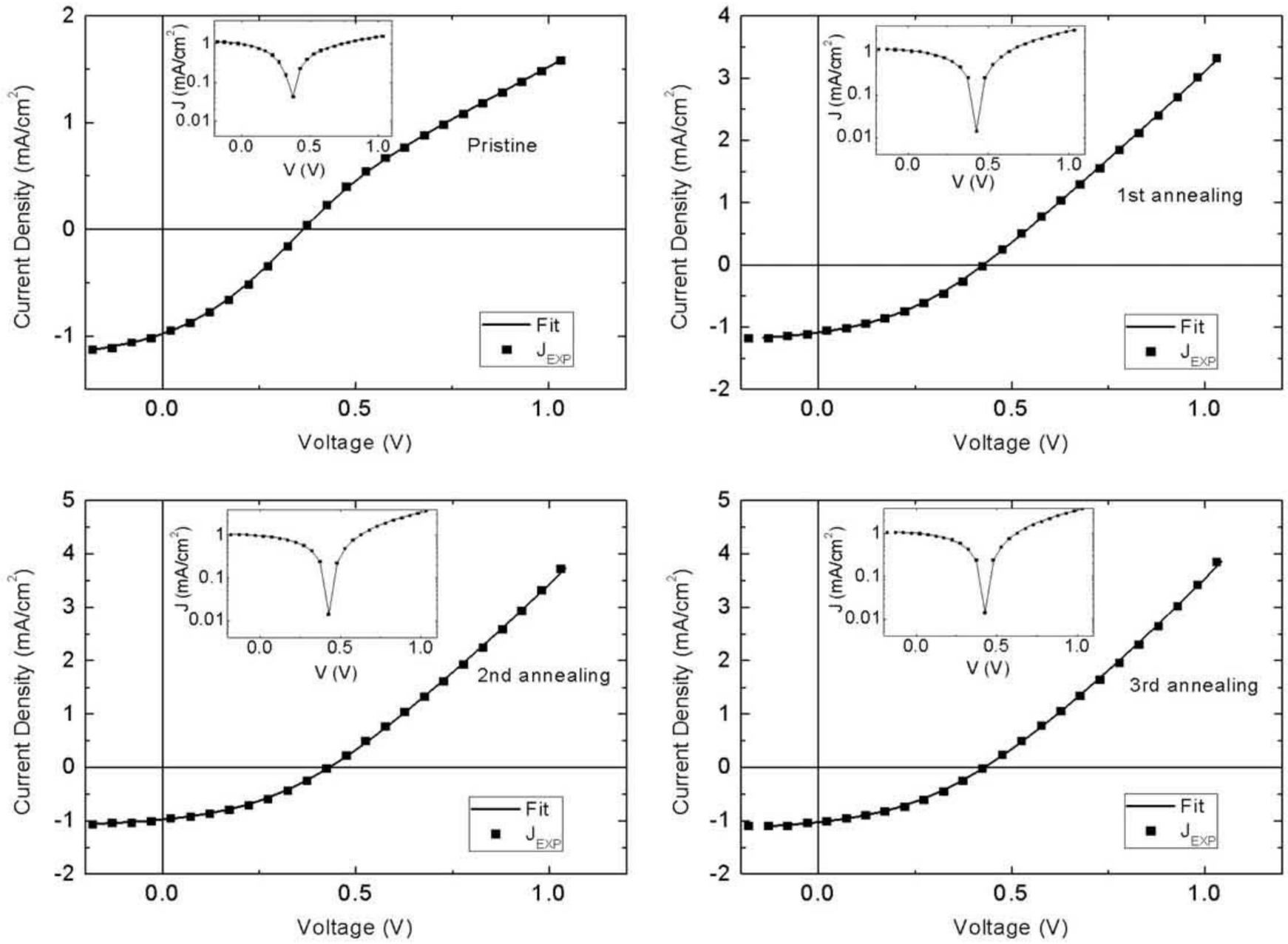

Fig. 5. Experimental (filled symbols) and theoretical (solid line) J–V curves for the pristine device and after three annealings. Insets show J–V curves in logarithmic scale.

Table 1
Circuit parameters, FF and PCE corresponding to pristine device and after three annealing process.

	J_{01} (mA cm ^{2})	J_{02} (mA cm ^{2})	R_{P1} (MΩ)	R_{P2} (kΩ)	FF	PCE (%)
Pristine	0.14	0.42	0.66	6.44	0.324	0.28
1st annealing	0.10	0.42	0.74	1.92	0.363	0.42
2nd annealing	0.08	0.38	10.10	1.55	0.383	0.40
3rd annealing	0.09	0.28	9.31	1.47	0.373	0.41

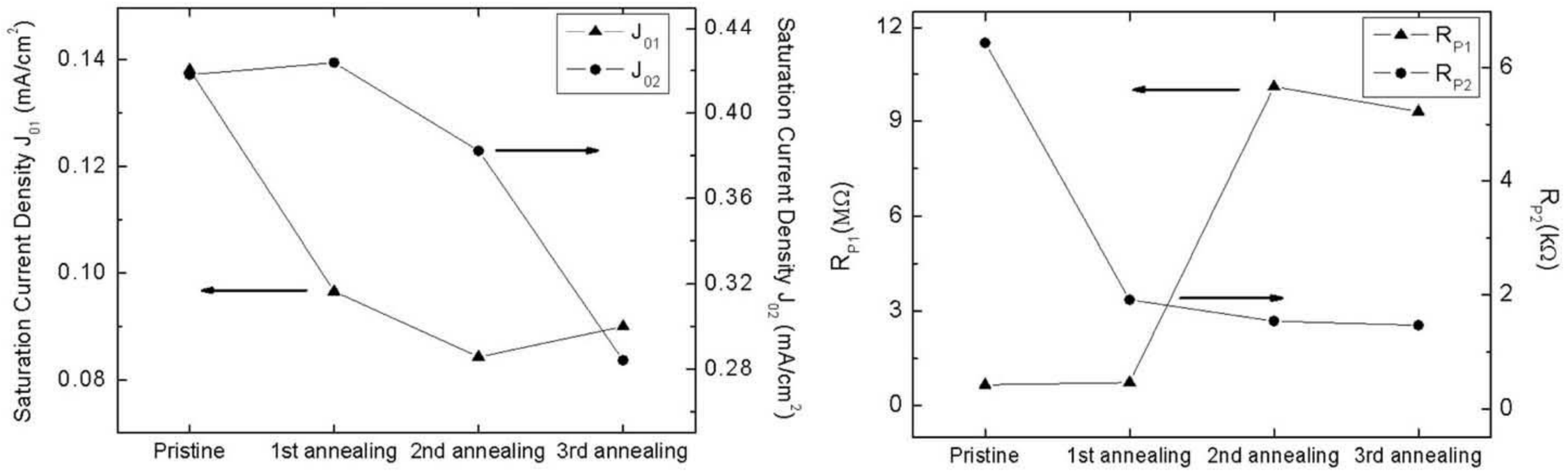

Fig. 6. Evolution of the saturation current densities J_{01} and J_{02} (left) and parallel resistances R_{P1} and R_{P2} (right) with the annealing treatment.

the main factor responsible for kink annihilation. The decrease in R_{P2} is also reflected in the increase of the J–V slope at high voltages. Evolution of the electric parameters is shown in Fig. 6. These tendencies agree well with the hypothesis of an improvement of the organic/cathode interface during annealing.

On the other hand, R_{P1} increases from 0.66 MΩ to 9.31 MΩ which indicates a strong reduction of current leakages, which improves the performance of the solar cell.

4. Conclusions

In this work we have studied the evolution of the S-shape appearing in the J–V curves of organic solar cells with annealing from a theoretical and experimental point of view. The kink appearing in pristine devices has been removed after undergoing repetitive slow annealing processes. In order to model the electrical characteristics of organic solar cells showing S-shape

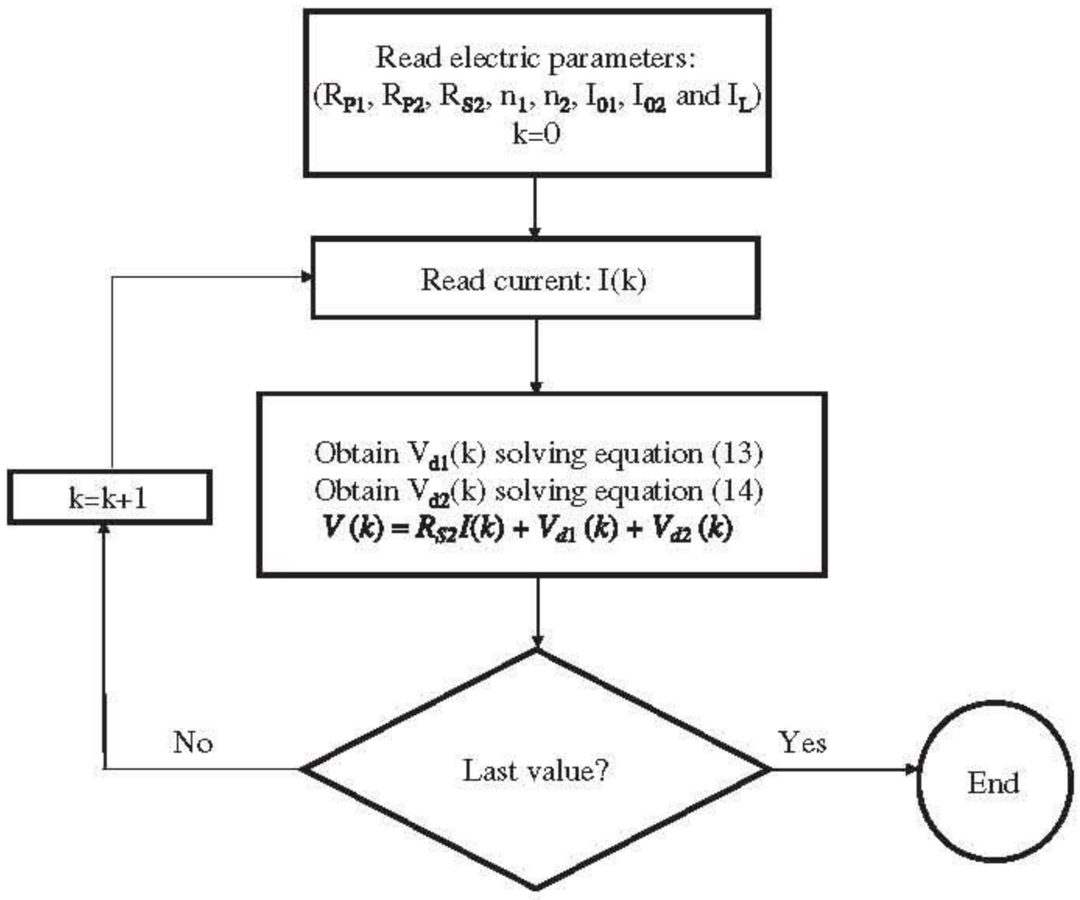

Fig. A1. Flow diagram used to solve electric circuit.

we have numerically solved, without approximations, the transcendental equation system derived from an equivalent circuit that reproduces the kink.

Values of R_{P2}, R_{P1}, J_{02} and J_{01} have been extracted for pristine and annealed devices, indicating that a strong decrease in R_{P2} from 6.44 kΩ to 1.47 kΩ is responsible for the kink annihilation, readily observed in the first annealing. Consecutive annealings results in simultaneous decreasing in J_{02} and R_{P2}, attenuating the second diode effect and ultimately removing the kink shape.

Acknowledgments

This work has been supported by the Comunidad Autónoma de Madrid and the Universidad Rey Juan Carlos under Project Nos. S2009/ESP-1781 and URJC-CM-2010-CET-5173.

Appendix A

See Fig. A1.

References

[1] H. Shirakawa, E.J. Louis, A.G. MacDiarmid, C.K. Chiang, A.J. Heeger, Synthesis of electrically conducting organic polymers–halogen derivatives of polyacetylene, $(CH)_x$, Journal of the Chemical Society Chemical Communications 16 (1977) 578–580.
[2] S. Sariciftci, L. Smilowitz, A.J. Heeger, F. Wudl, Photoinduced electron transfer from a conducting polymer to buckminsterfullerene, Science 258 (1992) 1474–1476.
[3] M. Reyes-Reyes, K. Kim, D.L. Carroll, High-efficiency photovoltaic devices based on annealed poly(3-hexylthiophene) and 1-(3-methoxycarbonyl)-propyl-1-phenyl-(6,6)C61 blends, Applied Physics Letters 87 (2005) 083506.
[4] K. Lee, J.Y. Kim, S.H. Park, S.H. Kim, S. Cho, A.J. Heeger, Air-stable polymer electronic devices, Advanced Materials 19 (2007) 2445–2449.
[5] G. Li, V. Shrotriya, J. Huang, Y. Yao, T. Moriarty, K. Emery, Y. Yang, High-efficiency solution processable polymer photovoltaic cells by self-organization of polymer blends, Nature Materials 4 (2005) 864–868.
[6] J.Y. Kim, K. Lee, N.E. Coates, D. Moses, T.-Q. Nguyen, M. Dante, A.J. Heeger, Efficient tandem polymer solar cells fabricated by all-solution processing, Science 317 (2007) 222–225.
[7] H. Hoppe, N.S. Sariciftci, Morphology of polymer/fullerene bulk heterojunction solar cells, Journal of Materials Chemistry 16 (2006) 45–61.
[8] S.C. Veenstra, J. Loos, J.M. Kroon, Nanoscale structure of solar cells based on pure conjugated polymer blends, Progress in Photovoltaics: Research and Applications 15 (2007) 727–740.
[9] Soheil Ebadian, Bobak Gholamkhass, Shabnam Shambayati, Steven Holdcroft, Peyman Servati, Effects of annealing and degradation on regioregular polythiophene-based bulk heterojunction organic photovoltaic devices, Solar Energy Materials & Solar Cells 94 (2010) 2258–2264.
[10] Golap Kalita, Matsushima Masahiro, Wakita Koichi, Masayoshi Umeno, Nanostructured morphology of P3HT:PCBM bulk heterojunction solar cells, Solid-State Electronics 54 (2010) 447–451.
[11] L.H. Nguyen, H. Hoppe, T. Erb, S. Günes, G. Gobsch, N.S. Sariciftci, Effects of annealing on the nanomorphology and performance of poly(alkylthiophene):fullerene bulk-heterojunction solar cells, Advanced Functional Materials 17 (2007) 1071–1078.
[12] M.M. Mandoc, W. Veurman, J. Sweelssen, M.M. Koetse, P.M. Blom, Origin of the efficiency improvement in all-polymer solar cells upon annealing, Applied Physics Letters 91 (2007) 073518.
[13] M. Vogel, S. Doka, Ch. Breyer, M. Ch., Lux-Steiner, K. Fostiropoulos, On the function of a bathocuproine buffer layer in organic photovoltaic cells, Applied Physics Letters 89 (2006) 163501.
[14] Iván Mora-Seró, Juan Bisquert, Effect of reduced selectivity of contacts on the current–potential characteristics and conversion performance of solar cells, Solar Energy Materials & Solar Cells 85 (2005) 51–62.
[15] Matthew O. Reese, Matthew S. White, Garry Rumbles, David S. Ginley, Sean E. Shaheen, Optimal negative electrodes for poly(3-hexylthiophene): [6,6]-phenyl C61-butyric acid methyl ester bulk heterojunction photovoltaic devices, Applied Physics Letters 92 (2008) 053307.
[16] Dhritiman Gupta, Monojit Bag, K.S. Narayan, Correlating reduced fill factor in polymer solar cells to contact effects, Applied Physics Letters 92 (2008) 093301.
[17] Dhritiman Gupta, Sabyasachi Mukhopadhyay, K.S. Narayan, Fill factor in organic solar cells, Solar Energy Materials & Solar Cells 94 (2010) 1309–1313.
[18] Ankit Kumar, Srinivas Sista, Yang Yang, Dipole induced anomalous S-shape I–V curves in polymer solar cells, Journal of Applied Physics 105 (2009) 094512.
[19] Fernando Araujo de Castro, Jakob Heier, Frank Nüesch, Roland Hany, Origin of the kink in current–density versus voltage curves and efficiency enhancement of polymer-C60 heterojunction solar cells, IEEE Journal of Selected Topics in Quantum Electronics 16 (2010) 1690–1699.
[20] M. Glatthaara, M. Riede, N. Keegan, K. Sylvester-Hvid, B. Zimmermann, M. Niggemanna, A. Hinsch, A. Gombert, Efficiency limiting factors of organic bulk heterojunction solar cells identified by electrical impedance spectroscopy, Solar Energy Materials & Solar Cells 91 (2007) 390–393.
[21] Mathilde R. Lilliedal, Andrew J. Medford, Morten V. Madsen, Kion Norrman, Frederik C. Krebs, The effect of post-processing treatments on inflection points in current–voltage curves of roll-to-roll processed polymer photovoltaics, Solar Energy Materials & Solar Cells 94 (2010) 2018–2031.
[22] Frederik C. Krebs, Kion Norrman, Analysis of the failure mechanism for a stable organic photovoltaic during 10,000 h of testing, Progress in Photovoltaics: Research and Applications 15 (2007) 697–712.
[23] Jan Alstrup, Mikkel Jørgensen, Andrew J. Medford, Frederik C. Krebs, Ultra fast and parsimonious materials screening for polymer solar cells using differentially pumped slot-die coating, ACS Applied Materials and Interfaces 2 (2010) 2819–2827.
[24] Q.L. Song, F.Y. Li, H. Yang, H.R. Wu, X.Z. Wang, W. Zhou, J.M. Zhao, X.M. Ding, C.H. Huang, X.Y. Hou, Small-molecule organic solar cells with improved stability, Chemical Physics Letters 416 (2005) 42–46.
[25] Wolfgang Tress, Annette Petrich, Markus Hummert, Moritz Hein, Karl Leo, Moritz Riede, Imbalanced mobilities causing S-shaped I–V curves in planar heterojunction organic solar cells, Applied Physics Letters 98 (2011) 063301.
[26] Simon M. Sze, Physics of Semiconductor Devices, 3rd ed., John Wiley & Sons, Inc., 2007.
[27] Seunghyup Yoo, Benoit Domercq, Bernard Kippelen, Intensity-dependent equivalent parameters of organic solar cells based on pentacene and C60, Journal of Applied Physics 97 (2005) 103706.
[28] Ali Cheknane, Hikmat S. Hilal, Fayc- al Djeffal, Boumediene Benyoucef, Jean-Pierre Charles, An equivalent circuit approach to organic solar cell modelling, Microelectronics Journal 39 (2008) 1173–1180.
[29] Chunfu Zhang, Jincheng Zhang, Yue Hao, Zhenhua Lin, Chunxiang Zhu, A simple and efficient solar cell parameter extraction method from a single current–voltage curve, Journal of Applied Physics 110 (2011) 064504.
[30] Ken-ichi Ishibashi, Yasuo Kimura, Michio Niwano, An extensively valid and stable method for derivation of all parameters of a solar cell from a single current–voltage characteristic, Journal of Applied Physics 103 (2008) 094507.
[31] Amit Jain, Avinashi Kapoor, A new approach to study organic solar cell using Lambert W-function, Solar Energy Materials & Solar Cells 86 (2005) 197–205.
[32] Adelmo Ortiz-Conde, Francisco J. García Sánchez, Juan Muci, New method to extract the model parameters for solar cells from the explicit analytic solutions of their illuminated I–V characteristics, Solar Energy Materials & Solar Cells 90 (2006) 352–361.
[33] Avinashi Kapoor, Amit Jain, Exact analytical solutions of the parameters of real solar cells using Lambert W-function, Solar Energy Materials & Solar Cells 81 (2004) 269–277.
[34] B. Mazhari, An improved solar cell circuit model for organic solar cells, Solar Energy Materials & Solar Cells 90 (2006) 1021–1033.
[35] W.J. Potscavage Jr., A. Haldi, A. Sharma, B. Kippelen, Equivalent circuit model for organic single-layer diodes, Journal of Applied Physics 104 (2008) 064503.
[36] A. Bouhemadou, M. Chegaar, N. Nehaoua, Organic and inorganic solar cells parameters evaluation from single I–V plot, Energy Conversion and Management 49 (2008) 1376–1379.
[37] T. Bäck, U. Hammel, H.-P. Schwefel, Evolutionary computation: comments on the history and current state, IEEE Transactions on Evolutionary Computation 1 (1997) 3–17.